INORGANIC CHEMISTRY

FRONTIERS

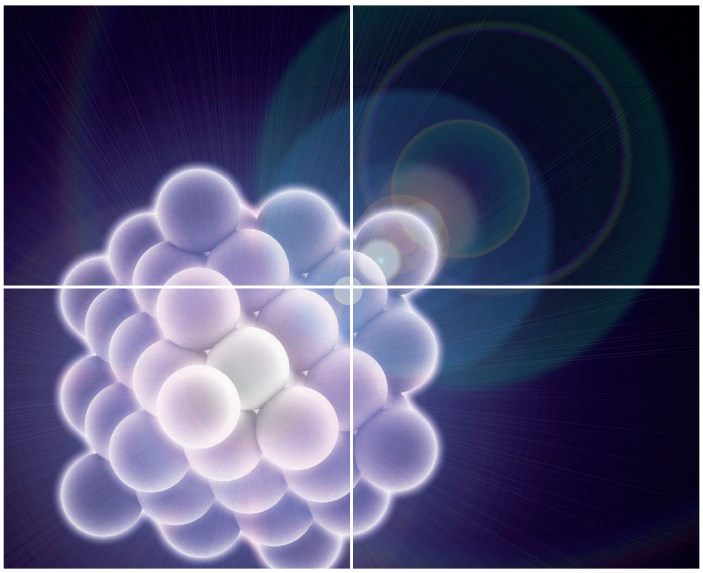

Accepted Manuscript

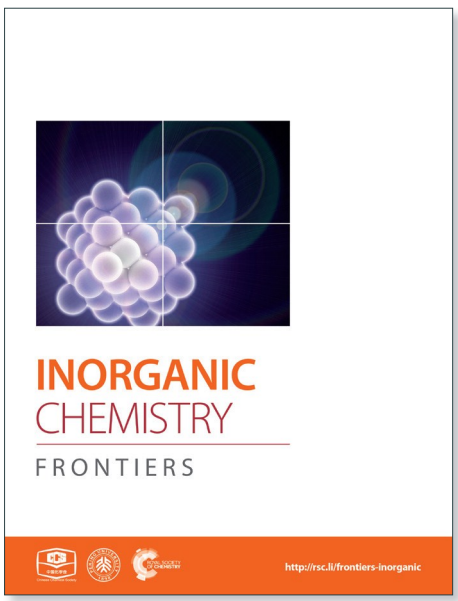

This is an *Accepted Manuscript*, which has been through the Royal Society of Chemistry peer review process and has been accepted for publication.

Accepted Manuscripts are published online shortly after acceptance, before technical editing, formatting and proof reading. Using this free service, authors can make their results available to the community, in citable form, before we publish the edited article. We will replace this *Accepted Manuscript* with the edited and formatted *Advance Article* as soon as it is available.

You can find more information about *Accepted Manuscripts* in the **Information for Authors**.

Please note that technical editing may introduce minor changes to the text and/or graphics, which may alter content. The journal's standard **Terms & Conditions** and the **Ethical guidelines** still apply. In no event shall the Royal Society of Chemistry be held responsible for any errors or omissions in this *Accepted Manuscript* or any consequences arising from the use of any information it contains.

Inorganic Chemistry Frontiers

ARTICLE

Phase and Morphology Evolution during the Solvothermal Synthesis of VO_2 Polymorphs

Received 00th January 20xx,
Accepted 00th January 20xx

DOI: 10.1039/x0xx00000x

www.rsc.org/

Liangmiao Zhang,[a]† Fang Xia,[b]† Zhengdong Song,[c] Nathan A. S. Webster,[d] Jingchao Song,[e,f] HongjieLuo[a,c] and Yanfeng Gao*[c]

The phase and morphological features of materials are often tunable by adjusting the reaction parameters of the solvothermal synthesis but this versatility also poses a challenge for preparing materials with desired phase and morphology if the behaviors of phase and morphological evolutions during the solvothermal synthesis are not known. In this work, the formation and growth of VO_2 nanomaterials in solvothermal systems via the reduction of V_2O_5 by ethylene glycol (EG) were investigated by in-situ powder X-ray diffraction (PXRD). The results show that both fast and slow heating produce the same VO_2(B) final product but the phase evolution during the synthesis is very sensitive to the heating rate. Fast heating (10 °C min^{-1}) invoives an unknown intermediate while $V_3O_7 \cdot H_2O$ is the intermediate phase at slow heating (2 °C min^{-1}). The formation mechanism was employed to design the synthesis of VO_2(B) nanorods and the phase transformation paths were verified by large-scale batch synthesis. Furthermore, ex-situ PXRD and SEM were employed to follow the structure and morphology evolution during growth. This research indicates that in-situ PXRD, as a powerful tool to monitor the whole reaction process and to collect information such as phase evolution and the fate of the transient intermediates, can be used to direct the controlled synthesis of materials.

1. Introduction

Vanadium dioxides (VO_2) is one of the most important metal oxides and has been widely studied and applied in the field of sensor,[1] catalyst,[2] smart window,[3] lithium-ion batteries,[4] and so on. To date, VO_2 is found to exhibit the richest family of crystalline polymorphs, such as thermodynamically stable VO_2(M), VO_2(R) phases and metastable VO_2(A), VO_2(B), VO_2(D), VO_2(P) phases, etc.[5] The distinguishing feature of each VO_2 polymorph is the arrangement scheme of edge- or corner-sharing VO_6 octahedra.[6] It is well known that the chemical and physical properties of nanomaterials are greatly influenced by the size, shape and crystal structure of the materials. Therefore, it is of paramount importance to understand the materials formation and growth behaviours and ultimately enable tailored synthesis of VO_2 with controllable phase, size and morphology.

Various physical and chemical methods have been employed to prepare vanadium dioxides, including chemical vapour deposition,[7] the ion implantation technique,[8] hydro/solvothermal growth,[9] sol-gel synthesis,[10] and precursor pyrolysis.[11] However, most of the methods are expensive, inefficient, and energy-intensive. Among the aforementioned methods, the hydro/solvothermal route is promising as it offers advantages of low cost, high yield, and is relatively environmentally benign. Selective formation of vanadium oxides with desired phase compositions can be achieved by hydrolysis of vanadium containing precursors,[12,13] reduction of pentavalent vanadium compounds (V_2O_5, NH_4VO_3) by reducing agents (oxalic acid,[14,15] PVP,[16] or EG[17]), and homogeneous precipitation of $VOSO_4$ with urea under mild hydro/solvothermal conditions.[18] The synthesis is very sensitive to reaction parameters such as temperature, solvent composition, precursor concentration, reaction time, pH value, and autoclave filling ratio.[19] As we know, tuning experimental parameters in a hydrothermal reaction system, various VO_2 polymorphs can be successfully synthesized. Nevertheless, the interplay between these parameters is complicated, and hence the synthesis of vanadium oxides with desired composition often requires many 'trial and error' experiments and strictly controlled condition. Although a number of reaction mechanisms have been proposed, they are based on ex-situ characterization and little direct evidence has been gathered for the phase transformations and complex redox reactions that occurred under the hydro/solvothermal synthesis conditions. A clearer understanding of process is essential for more efficient and tailored synthesis of vanadium dioxides, and this requires in-situ monitoring of the hydro/solvothermal synthesis.

[a] Shanghai Institute of Ceramics (SIC), Chinese Academy of Sciences (CAS), 1295 Dingxi Rd., Shanghai 200050, China
[b] School of Engineering and Information Technology, Murdoch University, Murdoch, WA 6150, Australia
[c] School of Materials Science and Engineering, Shanghai University, 99 Shangda Rd., Shanghai 200444, China. E-mail: yfgao@shu.edu.cn
[d] CSIRO Mineral Resources, Private Bag 10, Clayton South, VIC 3169, Australia
[e] CSIRO Manufacturing, Clayton, VIC 3168, Australia
[f] Department of Materials Science and Engineering, Monash University, Clayton, VIC 3800, Australia

† These authors contributed equally to this work. Electronic Supplementary Information (ESI) available: In- situ SR-XRD patterns, images and movie captured by the surveillance camera, TEM images of samples prepared at 250 °C for 12h, crystal structure models of (a) V_3O_7, (b) VO_2(B) and (c) VO_2(D), and SEM and XRD of samples prepared with various molar ratios of EG: V_2O_5.
See DOI: 10.1039/x0xx00000x

In-situ PXRD offers such an opportunity to monitor the hydro/solvothermal synthesis and is able to provide a clear synthesis mechanism that can guide the batch autoclave synthesis. Compared with traditional ex-situ PXRD characterization, in-situ PXRD allows for observation of the short-lived intermediate phases which are often missed by ex-situ characterization. In-situ PXRD has been shown to be a powerful tool for understanding the hydro/solvothermal syntheses of a number of materials, including MnO_2,[20] colloid Au nanoparticles,[21] CoAPO-5 molecular sieves,[22] $Bi_2Se_xTe_{3-x}$ (x = 0~3) hexagonal nanoplatelets,[23] mesoporous TiO_2 beads,[24] WO_x-ethylenediaminenanowires,[25] γ/β-MnO_2[26] and VO_2(A).[5]

In this paper, we prepared various nano-VO_2 polymorphs by the reduction of V_2O_5 using ethylene glycol (EG) as the reducing agent. In order to understand the process involved, we employ in-situ PXRD to follow the phase evolution during the synthesis of VO_2 polymorphs via a redox reaction between V_2O_5 and EG. Clear phase transformation paths have been revealed. The obtained mechanism was used for the design of batch autoclave syntheses and the desired products were successfully prepared and characterized by ex-situ XRD, XPS, SEM and TEM. Moreover, the intermediate phases were captured by ex-situ PXRD and the morphology evolution process was investigated by ex-situ SEM.

2. Experimental Section

2.1 In-situ PXRD experiments

One synchrotron-based in-situ PXRD (SB-PXRD) experiment was conducted on the powder diffraction beamline at the Australian Synchrotron and another laboratory-based in-situ PXRD (LB-PXRD) experiment was carried out using an Inel EQUINOX 3000 instrument at CSIRO Mineral Resources. For the SB-PXRD experiment, X-ray wavelength (λ =0.6889Å) was calibrated using a LaB_6 standard (NIST SRM 660b). For the LB-PXRD experiment, Mo Ka radiation (λ = 0.7093 Å) from a tube operated at 40kV and 40mA was used. The sample presentation setups used in SB-PXRD and LB-PXRD experiments were the same and have been described in detail elsewhere.[5, 23-25] The starting precursor (homogenized mixture of 0.25 g V_2O_5, 0.077 mL EG and 1.331 mL Milli-Q water) was injected into a quartz glass capillary (1 mm in outer diameter, 0.1 mm in wall thickness, and 40 mm in length), which was then fitted to a custom-made stainless steel holder. 4 MPa and 3 MPa external N_2 pressures were applied to the capillary during the synthesis to prevent oxidation and boiling of the solvent in the SB-PXRD and LB-PXRD experiments, respectively. The slurry-containing capillary was fixed at the X-ray beam center and was heated to synthesis temperature by a hot air blower beneath the capillary. To study the effect of heating rate on the syntheses mechanism, a fast heating rate (10 ^oC min^{-1}) was used in the SB-PXRD experiment, while a slower heating rate (2 ^oC min^{-1}) was used in the LB-PXRD experiment. The temperature was monitored by a K-type thermocouple located 3.5 mm beneath the capillary and in the stream of hot air. In-situ PXRD patterns were collected continuously during the synthesis, with individual datasets collected for ~ 2 min. The detectors for both the SB-PXRD and LB-PXRD experiments were wide-angle 1D detectors capable of collecting >80° 2θ simultaneously. The capillary was oscillated continuously during the measurements, which ensured temperature homogeneity and minimized potential effects of preferred orientation. In the LB-PXRD experiment, a surveillance camera was also used to monitor visual appearance of the contents in the capillary reaction vessel as the synthesis reactions progressed (Fig.S4).

2.2 Designed batch autoclave synthesis

The synthesis mechanism obtained from in-situ PXRD was used to design the large scale synthesis using conventional laboratory autoclaves. The samples from autoclaves syntheses also provided an opportunity to study the morphological evolution during the syntheses. Typically, 20 mL deionized water was mixed with 0.43 mL EG. Subsequently, 1.41 g V_2O_5 was added into the mixed solvent with continuous magnetic stirring to form an orange suspension. The mixture was then transferred into a 25 mL Teflon-lined stainless steel autoclave. The autoclave was heated at the designed temperature for several hours and cooled down to room temperature naturally. The as-prepared powders were separated by centrifugation, washed with distilled water and absolute ethanol several times and dried under vacuum at 60 ^oC in an oven over night.

2.3 Ex-situ characterization

The morphology of the as-prepared batch autoclave samples was examined using field-emission scanning electron microscopy (FESEM, JSM-6700F, JEOL, Japan) and high-resolution transmission electron microscopy (TEM, JEM-2010F, JEOL). The phase structure was identified using PXRD on a Rigaku D/Max-RB X-ray diffractometer with Cu Kα radiation (λ=1.5418 Å). X-ray photoelectron spectroscopy (XPS) spectra were collected on a VG ESCALAB MK II system equipped with Al KR radiation as the X-ray source.

3. Results and Discussion

3.1 In-situ PXRD characterization

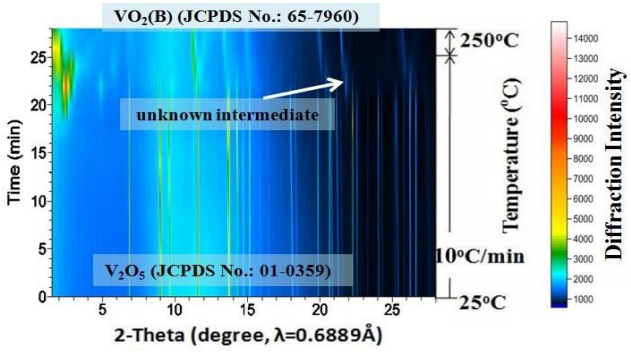

Fig. 1 Accumulated time-resolved in-situ SB-PXRD patterns (viewed down the intensity axis) collected during the synthesis at 250 ^oC with a heating rate of 10 ^oC min^{-1}.

Inorganic Chemistry Frontiers

ARTICLE

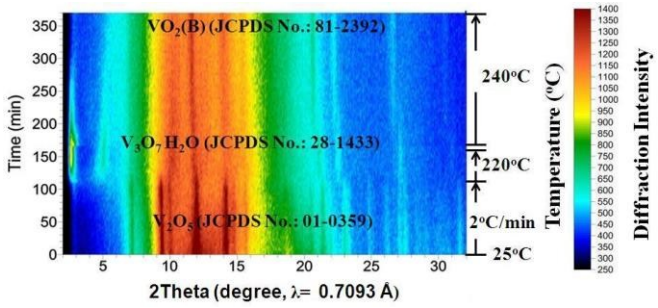

Fig. 2 Accumulated time-resolved in-situ LB-PXRD patterns (viewed down the intensity axis) collected during the synthesis at 240 °C with slow heating (2 °C min^{-1}).

The accumulated time-resolved in-situ SB-PXRD patterns viewed down the intensity axis, for synthesis of VO_x nanostructures with equivalent moles of EG and V_2O_5, are shown in Fig. 1. The SB-PXRD pattern of the starting material can be indexed to the orthorhombic phase of V_2O_5 (JCPDS card No.: 01-0359) (Fig.S1). When the heating rate was 10 ^oC min^{-1}, V_2O_5 transformed to a new compound in the temperature interval 210-240 ^oC, which does not match any vanadium oxide or hydrated vanadium oxide phase in the latest ICDD PDF database. Crystal structure could not be determined for this intermediate phase as the signal to noise ratio of the in situ diffraction pattern is not sufficiently high (Fig. S2). With further heating, the typical peaks of the intermediate faded very quickly. Meanwhile, the peaks of VO_2(B) (JCPDS card No.: 81-2392) (Fig.1 & S3) grew rapidly and the three strongest peaks appeared at 11.2°, 13. 4°, and 21.4°, corresponding to the (110), (111), and (020) lattice planes of the VO_2(B) crystallites, respectively.

Fig.2 shows the results of the in-situ LB-PXRD experiment, where a slower heating rate (2 ^oC min^{-1}) was employed. As shown in Fig.2, the peaks of monoclinic V_2O_5 (JCPDS card No.: 01-0359) precursor continuously diminish at 220 ^oC, until it is consumed to form the intermediate compound $V_3O_7{\cdot}H_2O$ (JCPDS card No.: 28-1433). In order to capture this phase in more detail, the temperature was maintained at 220 ^oC for 60 min, before the temperature was increased to 240 ^oC upon which the intermediate $V_3O_7{\cdot}H_2O$ was further reduced to the monoclinic VO_2(B) (JCPDS card No.: 81-2392).

Although the same final products (VO_2(B)) are obtained under fast and slow heating conditions, different intermediate phases are involved. As the reaction proceeds, the fraction of VO_2(B) increases at the expense of the intermediates. The in situ data reveal that the formation mechanism for VO_2(B) is highly dependent on heating rate. The reducing process from V_2O_5 to VO_2(B) with a reducing agent (EG) can be described as a two-step process from partial reduction−hydration to complete reduction and dehydration with the following equations:

Fast heating (10 °C min^{-1})

Step 1: $V_2O_5 + H_2O + EG \rightarrow$ unknown intermediate

Step 2: unknown intermediate $+ EG \rightarrow VO_2(B) + H_2O$

Slow heating (2 °C min^{-1})

Step 1: $V_2O_5 + H_2O + EG \rightarrow V_3O_7 \cdot H_2O$

Step 2: $V_3O_7 \cdot H_2O + EG \rightarrow VO_2(B) + H_2O$

Note that the above reactions are not balanced because the oxidation products of EG are unknown. As shown in the equations above, V_2O_5 and EG completely react with each other to form a reaction intermediate in the early stage of the reduction process. The intermediate is $V_3O_7 \cdot H_2O$ for the synthesis at 240 ^oC with a slow heating rate of 2 °C min^{-1}. The vanadium presents as a mixture of V(IV) and V(V). For fast heating (10 °C min^{-1}) at 250 ^oC, it is also likely that the vanadium presents as a mixture of V(IV) and V(V). As the reaction progresses, the remaining V(V) in the intermediate compound is further reduced, resulting in VO_2(B). The mechanisms determined here are quite different from the mechanism proposed by Pollet,[27] who reported the formation of the intermediate compound $VO_2{\cdot}xH_2O$ between $V_{10}O_{24}{\cdot}9H_2O$ and VO_2(B).

3.2 Designed batch autoclave synthesis

In-situ experiments give us the first-hand information about the synthesis in real time, and provide the basis for the design of batch autoclave synthesis. Batch autoclave synthesis of VO_2(B) was conducted using the same precursor, and at 220 ^oC for 12h with a heating rate of 4 °C min^{-1}. The chemical composition and phase structure of the as-synthesized powders were identified by PXRD and XPS, and the results are shown in Figs. 3 and 5e. All the diffraction peaks can be perfectly indexed to the monoclinic phase of VO_2(B) (JCPDS card, No.: 81-2392) (Fig.5e). The V2p peaks of the sample (Fig.3b) can be fitted to three main peaks centred at 516.2 and 523.6 eV, which corresponds to V^{4+} according to previous reports.[28] Therefore, the as-prepared materials are pure monoclinic VO_2(B).

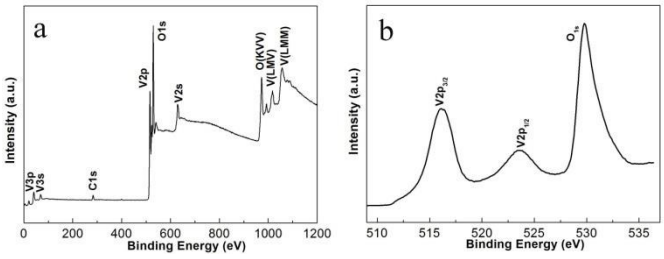

Fig. 3 XPS of VO_2(B) products (a) full survey spectrum; (b) core-level spectra of V_{2p} and O_{1s}.

The morphologies of the samples prepared at 220 ^oC for 12h were investigated using SEM and TEM. Fig.4a illustrates a representative SEM image of the as-prepared VO_2(B) materials. A

large quantity of uniform and well-dispersed nanorods were obtained with an average across-section dimension of 200 nm × 300 nm and an average length of ~ 1 μm. Fig. 4b shows the detailed morphology at the end of an individual nanorod, distinctly showing the round tip and smooth edge surface. Further inspection using high-resolution TEM (HRTEM) (Fig. 4d) reveals the well-resolved lattice fringes with an interplanar distance of 0.357 nm, in accordance with the spacing of (110) planes of VO_2(B). The corresponding selected area electron diffraction (SAED) pattern (Fig. 4c) taken from the area marked by red circle displays a regular diffraction pattern, further affirming the single-crystal nature of these nanorods. When the samples were synthezied at 250 °C for 12 h (heating rate=10 °C min^{-1}), VO_2(B) were also obtained (Fig. 5e), demonstrating the large-scale batch synthesis results agree well with the final phases observed in the in-situ experiments (Figs. 1 and 2). The TEM and SEM images (Figs. S5a, b & Figs. 6e) distinctly show the product consists of monodispersed nanorods and irregular nanoparticles. The interplanar distance of 0.357 nm matches well with the (110) plane spacing of monoclinic VO_2(B), which indicates a preferred growth direction along [001] of monoclinic VO_2(B). The corresponding SAED pattern (Fig. S5c) also reveals the crystalline nature of these nanorods.

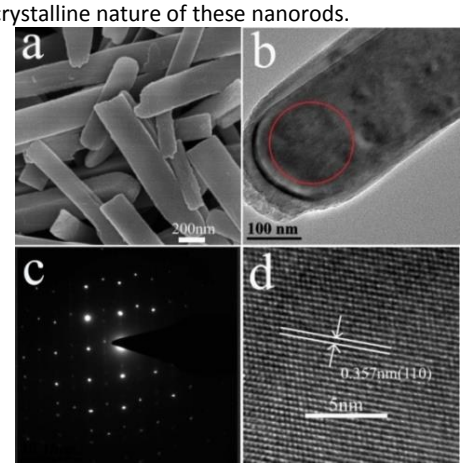

Fig. 4 (a) SEM and (b) TEM images of VO_2(B). (d) Its corresponding HRTEM image and (c) SAED pattern.

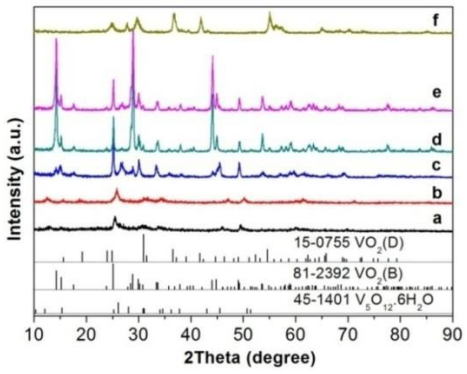

Fig. 5 PXRD patterns of samples prepared at 250 °C (heating rate=10 °C min^{-1}) for different times. (a) 1h, (b) 2h, (c) 3h, (d) 6h, (e) 12h, (f) 18h. The JCPDS patterns for V_5O_{12}·$6H_2O$, VO_2(B) and VO_2(D) are also shown. Patterns have been offset in the intensity axis for clarity.

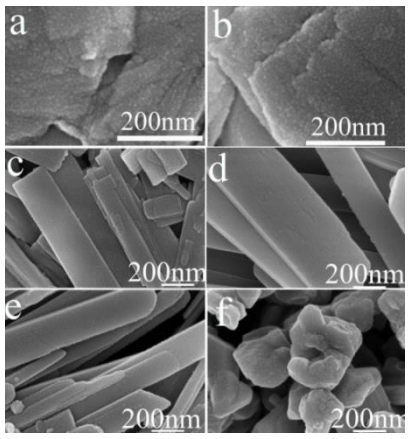

Fig. 6 SEM images of samples prepared at 250 °C (heating rate=10 °C min^{-1}) for various times. (a) 1h; (b) 2h; (c) 3h; (d) 6h; (e) 12h; (f) 18h.

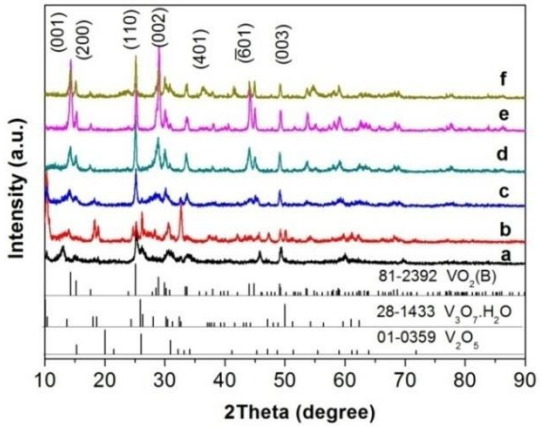

Fig. 7 PXRD patterns of samples prepared at 220 °C (heating rate=4 °C min^{-1}) for various times. (a) 1h, (b) 2h, (c) 3h, (d) 6h, (e) 12h, (f) 18h. The JCPDS patterns for V_2O_5, V_3O_7·H_2O and VO_2(B) are also shown. Patterns have been offset in the intensity axis for clarity.

3.3 Morphology and phase evolution

Both ex-situ and in-situ studies play important roles in understanding in detail the formation mechanism of materials. To further verify the in-situ PXRD results and monitor the morphology evolution, a series of time-dependent experiments were designed and carried out, and the products were characterized by ex-situ PXRD and SEM. When the reaction temperature was 220 °C (heating rate=4 °C min^{-1}), different morphologies were obtained with the reacting time increasing from 1 to 2, 3, 6, 12, and 18 h. The H_2O molecules rapidly intercalate into the interlayer of V_2O_5 resulting in V_3O_7·H_2O with a layer structure when the reactions were stopped after 1 and 2h (Fig. 7a, 7b). Most of the irregular V_2O_5 microparticles (Fig.8a) fused and combined together (Fig.8b) to form nanorods covered on the surface of the original V_2O_5 microparticles, as shown in Fig.8c and d. With the increase of the reaction time to 3, 6 and 12 h, abundant uniform nanorods were obtained and grown longer and thicker (Fig. 8e-j). If the reaction was terminated at 18 h, some nanorods broke and cavities were developed on the surface (Fig. 8k, l). The typical VO_2(B) spheres

with inner hollow structures emerged in the product, which are shown by a white arrow in Fig. 8l. Simultaneously, the samples transformed from a mixture of $V_3O_7{\cdot}H_2O$ and VO_2(B) to pure VO_2(B) (Fig. 7c-f). When the reaction temperature was 250 °C (heating rate=10 °C min^{-1}), an obvious phase-forming sequence was observed: V_2O_5 to layered $V_5O_{12}{\cdot}6H_2O$ assembled with nanocrystals and then to VO_2(B) nanorods (Fig. 5, 6). It is most likely that the unknown intermediate phase which was detected by in situ PXRD is only stable at the solvothermal synthesis condition and this is why a different reaction intermediate $V_5O_{12}{\cdot}6H_2O$ was detected by ex situ PXRD. When the reaction time was further increased to 18h, the VO_2(D) phase formed (Fig.5f). Accordingly, the nanorods formed initially were broken completely into irregular nanoparticles with deep cavities (Fig.6f).

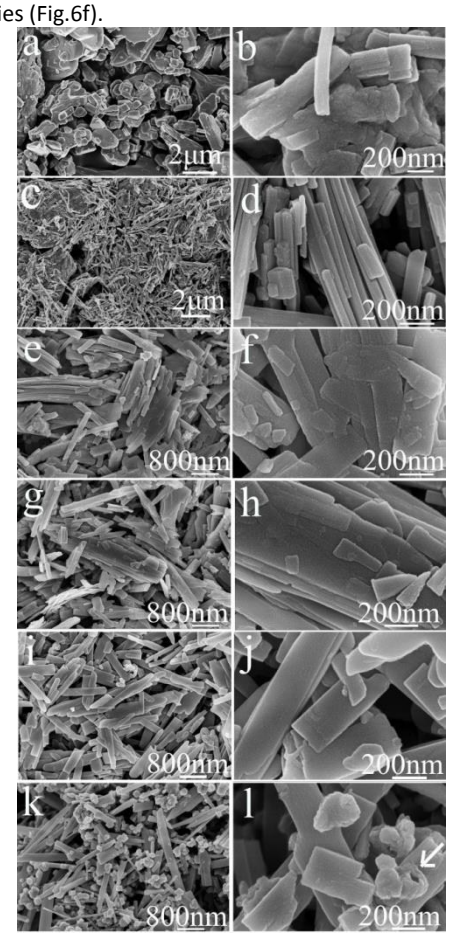

Fig. 8 SEM images of (a) V_2O_5 and the products prepared at 220 °C (heating rate=4 °C min^{-1}) for different times. (b) 1h; (c, d) 2h; (e, f) 3h; (g, h) 6h; (i, j) 12h; (k, l) 18h.

It was also found that the reaction temperature has a significant influence on the morphology and phase evolution. Figs. 9a, b, e, f show SEM images of VO_2 materials prepared by autoclaving the V_2O_5 and EG at different temperatures with a constant holding time of 24 h; their corresponding PXRD patterns are reported in Figs. 9c, d, g, h. It can be seen that aligned VO_2(B) nanorods with diameters of 40 ~ 80 nm and lengths up to 1 μm were obtained at 180 °C (Figs. 9a, c).These nanorods grew in size with increasing temperatures. At a higher temperature of 240 °C, nanorods intersected with each other and quite a few etched polyhedra were obtained. With a further increase in temperature to 260 °C, homogeneous VO_2(D) nano-dodecahedrons with open holes were observed, as shown in Fig.9f, which suggests that the as-obtained VO_2(D) nano-dodecahedrons with unique architecture are monodispersed and in high yield. All in all, further increasing the temperature or prolonging the reaction time, VO_2(D) may be formed, but they are not observed by the in-situ PXRD due to its long generation time. Usually, more than ten hours are required to obtain the pure VO_2(D) phase.

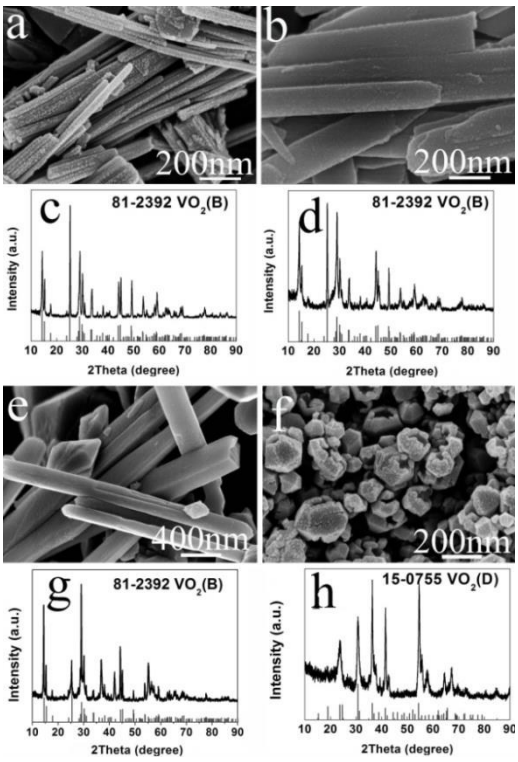

Fig. 9 SEM images and their corresponding PXRD patterns of samples prepared at different temperatures for 24h. (a, c) 180 °C; (b, d) 200 °C; (e, g) 240 °C; (f, h) 260 °C.

EG has been extensively used as a solvothermal solvent for the synthesis of vanadium oxide nanomaterials with hierarchical structure. [2,14,17,29] For example, Du and coworkers[17] have synthesized V_4O_7 hierarchical structures in a water-EG mixed medium by simply adjusting the amount of water in the EG solvent. Qian and coworkers[30] have prepared VO_2(B) nanowire arrays by reduction of V_2O_5 in a pure EG solvent. Cao and coworkers[31] have fabricated nanostructured V_2O_5 hollow microspheres by calcinations of vanadyl glycolate precursors formed also in pure EG solvent. The morphologies and phases of VO_2 are reported to be extremely dependent on the reaction temperature and time. When the reaction temperature is varied, the physical and chemical properties of the solvent such as density, viscosity, dielectric constant, ionic product can change. Thus, the reactivity, solubility, and diffusion rate of the reagents and intermediates can be greatly influenced, leading to various morphologies and structures of products. On the basis of in-situ and ex-situ results, a plausible formation mechanism for the formation of various VO_2 polymorphs can be illustrated in Scheme 1. Under solvothermal synthesis condition, irregular V_2O_5 particles, exhibiting layers of edge- and corner-sharing VO_5 square pyramids,[32] are initially reduced and

fused into layered hydrated vanadium oxide intermediate compounds, with the vanadium presenting as a mixture of V(IV) and V(V). The very loose stacked V-O layers in the intermediate phases endow the ability to insert guest species of H_2O between the interlayers of these materials (Fig.S6a). Further reduction results in reassembly into VO_2(B) nanorods growing along a preferred orientation [001]. As time elapses further, the well formed structure is broken, and the irregular nanoparticles reassemble into hollow dodecahedrons, hollow spheres or particles of VO_2(B) (Fig.S6b) or VO_2(D) (Fig.S6c). These nanostructures contain deep cavities and the inside- out Ostwald ripening may be responsible for the controllable growth of these hollow structures. A similar formation process has also been reported for the synthesis of AlOOH hollow core-shell microspheres,[33] hollow VO_2 microspheres[34]and SnO_2 hollow nanospheres,[35] etc. As reported by previous theoretical computation,[36-38] the formation energy of VO_2(D) is similar to the stable VO_2(R) phase, and is lower than that of VO_2(B). Therefore, the transformation from monoclinic VO_2(B) phase to VO_2(D) is driven by thermodynamics.

We also found that the formation of VO_x polymorphs strongly depends on the molar ratios of EG to V_2O_5. As for the lower EG content, a microemulsion system formed, the morphology is greatly dependent on the shape of the emulsion. When the molar ratio of EG to V_2O_5 was changed, the volume ratio of EG to water was changed accordingly. The lower molar ratios favour the formation of VO_2(B) nanorods or mixture of V_2O_3 and V_5O_9 phases with plate-like morphology (Fig.10a,d). When the molar ratio is increased to 4 or above, spherical V_2O_3 nanoparticles with a narrow size distribution of 15~30 nm are the dominant products (Fig.10b-d). Their detailed formation mechanism needs further study.

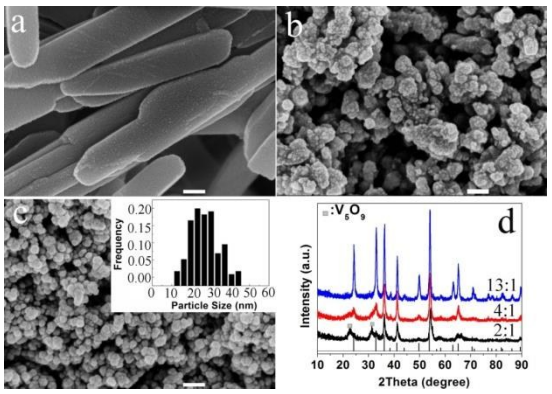

Fig. 10 (a-c) SEM images of samples prepared with various molar ratio of EG: V_2O_5 (2:1, 4:1, 13:1) at 260 °C for 4 h. The scale bar is 100 nm. The inset figure in c is the particle size distribution. (d) Their corresponding XRD patterns.

4. Conclusions

In summary, two in situ PXRD experiments demonstrate the phase evolution process during the solvothermal synthesis of VO_2(B) nanorods through a facile solvothermal reduction of V_2O_5 by EG. These results were used to guide the ex-situ batch autoclave synthesis. In addition, various VO_x polymorphs including nanorods, nanospheres and hollow nanododecahedrons can be successfully synthesized. The phase and morphology of these products can be tailored by simply adjusting the reaction time, temperature and molar ratio of EG to V_2O_5. The instructive and meaningful results may help understanding the formation mechanism on fundamental aspects during the hydro/solvothermal synthesis and improving the controlled synthesis technologies of vanadium oxide and other nanomaterials. Our ongoing research will focus on the underlying phase transformation based on structure analysis and their applications as catalysts, sensors or electrode materials, etc.

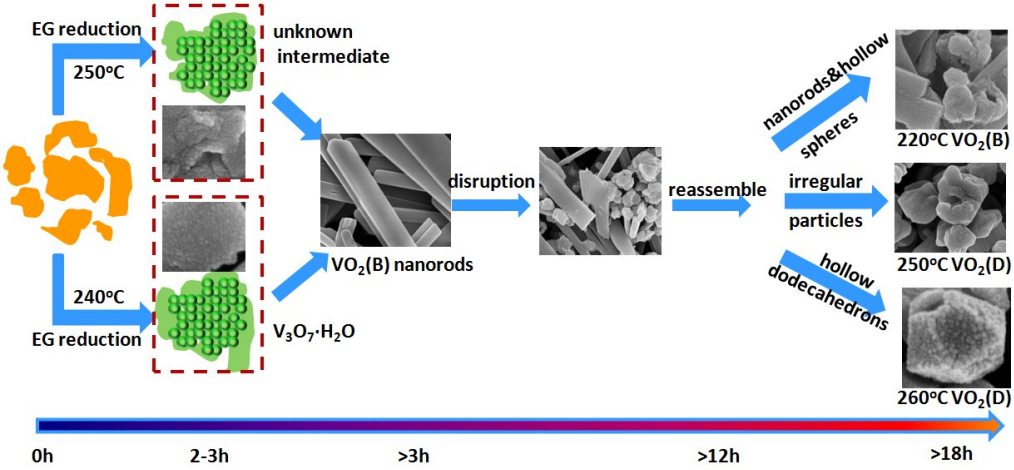

Scheme 1. Schematic representation of the evolution process for various VO_2 polymorphs formation.

Inorganic Chemistry Frontiers

ARTICLE

Acknowledgements

The authors are grateful for the financial support from the National Natural Science Foundation of China (51172265 and 51325203), the Ministry of Science and Technology of China (2014AA032802), the Science and Technology Commission of Shanghai Municipality (13521102100), the Education Commission of Shanghai Municipal (14ZZ099), the Guangdong Provincial Department of Science and Technology (2011A091104001), the Materials Genome Institute of Shanghai University (14DZ2261200) and the China Postdoctoral Science and Foundation (2014M561528). This research was partially undertaken on the powder diffraction beamline at the Australian Synchrotron, Victoria, Australia, through the Science and Industry Endowment Fund Special Research Program-Synchrotron Science. We thank Dr. Helen Brand and Dr. Justin Kimpton for beamline setup.

Notes and references

1 G. D. Nie, L. Zhang, J. Y. Lei, L. Yang, Z. Zhang, X. F. Lu and C. Wang, *J. Mater. Chem. A*, 2014, **2**, 2910.
2 X. Chen, F. Wang and J. Xu, *Top Catal.*, 2011, **54**, 1016.
3 Y. F. Gao, H. J. Luo, Z. T. Zhang, L. T. Kang, Z. Chen, J. Du, M. Kanehira and C. X. Cao, *Nano Energy*, 2012, **1**, 221.
4 C. Z. Wu and Y. Xie, *Energy Environ. Sci.*, 2010, **3**, 1191.
5 L. M. Zhang, F. Xia, Z. D. Song, N. A. S. Webster, H. J. Luo and Y. F. Gao, *RSC Adv.*, 2015, **5**, 61371.
6 L. Dai, Y. F. Gao, C. X. Cao, Z. Chen, H. J. Luo, M. Kanehira, J. Jin and Y. Liu, *RSC Adv.*, 2012, **2**, 5265.
7 Z. J. Li, Z. P. Hu, J. Peng, C. Z. Wu, Y. C. Yang, F. Feng, P. Gao, J. L. Yang and Y. Xie, *Adv. Funct. Mater.,* 2014, **24**, 1821.
8 R. Lopez and L. A. Boatner, *Phys. Rev. B: Condens. Matter Mater. Phys.*, 2002, **65**, 224113.
9 C. Z. Wu, F. Feng and Y. Xie, *Chem. Soc. Rev.*, 2013, **42**, 5157.
10 O. Berezina, D. Kirienko and A. Pergament, *Thin Solid Film,* 2015, **574**, 15.
11 N. Peys, P. Adriaensens, S. V. Doorslaer, S. Gielis, E. Peeters, C. D. Dobbelaere and S. D. Gendt, A. Hardy and M. K. V. Bael, *Dalton Trans.*, 2014, **43**, 12614.
12 Y. F. Sun, B. Y. Qu, S. S. Jiang, C. Z. Wu, B. C. Pan and Y. Xie, *Nanoscale*, 2011, **3**, 2609.
13 Y. F. Sun, S. S. Jiang, W. T. Bi, R. Long, X. G. Tan, C. Z. Wu, S. Q. Wei and Y. Xie, *Nanoscale*, 2011, **3**, 4394.
14 C. J. Niu, J. S. Meng, C. H. Han, K. N. Zhao, M. Y. Yan and L. Q. Mai, *Nano Lett.,* 2014, **14**, 2873.
15 G. P. Nagabhushana and G. T. Chandrappa, *J. Mater. Chem. A,* 2013, **1**, 11539.
16 M. Li, F. Y. Kong, L. Li, Y. X. Zhang, L. Chen, W. W. Yan and G. H. Li, *Dalton Trans*., 2011, **40**, 10961.
17 X. R. Wang, S. L. Zheng, X. C. Mu, Y. Zhang and H. Du, *Chem. Commun.,* 2014, **50**, 6775.
18 W. J. Li, S. D. Ji, Y. M. Li, A. B. Huang, H. J. Luo and P. Jin, *RSC Adv.,* 2014, **4**, 13026.
19 J. H. Jung, C. Y. Chen, W. W. Wu, J. Hong, B. K. Yun, Y. S. Zhou, N. Lee, W. Jo, L. J. Chen, L. J. Chou and Z. L. Wang, *J. Phys. Chem. C,* 2012, **116**, 22261.
20 X. F. Shen, Y. S. Ding, J. C. Hanson, M. Aindow and S. L. Suib, *J. Am. Chem. Soc.*, 2006, **128**, 4570.
21 S. Peng, J. S. Okasinski, J. D. Almer, Y. Ren, L. Wang, W. G. Yang and Y. G. Sun, *J. Phys. Chem. C,* 2012, **116**, 11842.
22 D. Grandjean, A. M. Beale, A. V. Petukhov and B. M. Weckhuysen, *J. Am. Chem. Soc.*, 2005, **127**, 14454.
23 J. Song, F. Xia, M. Zhao, Y. L. Zhong, W. Li, K.P. Loh, R. A. Caruso and Q. Bao, *Chem. Mater.*, 2015, **27**, 3471.
24 F. Xia, D. Chen, N. V. Y. Scarlett, I. C. Madsen, D. Lau, M. Leoni, J. Ilavsky, H. E. A. Brand and R. A. Caruso, *Chem. Mater.*, 2014, **26**, 4563.
25 W. Li, F. Xia, J. Qu, P. Li, D. Chen, Z. Chen, Y. Yu, Y. Lu, R. A. Caruso and W. Song, *Nano Res.*, 2014, **7**, 903.
26 T. Gao, H. Fjellvåg and P. Norby, *Nanotechnology,* 2009, **20**, 055610.
27 S. R. Popuri, M. Miclau, A. Artemenko, C. Labrugere,A. Villesuzanne and M. Pollet, *Inorg. Chem.,* 2013, **52**, 4780.
28 L. Liu, T. Yao, X. G. Tan, Q. H. Liu, Z. Q. Wang, D. C. Shen, Z. H. Sun, S. Q. Wei and Y. Xie, *small,* 2012, **8**, 3752.
29 Q. Ji, Y. C. Jiang, Z. P. Zhang, Y. T. Tian and Z. Y. Wang, *Z. Anorg. Allg. Chem.,* 2014, **640**, 1965.
30 X. Y. Chen, X. Wang, Z. H.Wang, J. X. Wan, J. W. Liu and Y. T. Qian, *Nanotechnology,* 2004, **15**, 1685.
31 E. Uchaker, N. Zhou, Y. W. Li and G. Z. Cao, *J. Phys. Chem. C,* 2013, **117**, 1621.
32 M. Winter, J. O. Besenhard, M. E. Spahr and P. Novák, *Adv. Mater.,* 1998, **10**, 725.
33 L. M. Zhang, W. C. Lu, R. R. Cui and S. S. Shen, *Mater. Res. Bull.*, 2010, **45**, 429.
34 F. Y. Kong, M. Li, X. Y. Yao, J. M. Xu, A. D. Wang, Z. P. Liu and G. H. Li, *CrystEngComm*, 2012, **14**, 3858-3861.
35 X. W. Lou, Y. Wang, C. Yuan, J. Y. Lee and L. A. Archer, *Adv. Mater.*, 2006, **18**, 2325.
36 L. Liu, F. Cao, T. Yao, Y. Xu, M. Zhou, B. Y. Qu, B. C. Pan, C. Z. Wu, S. Q. Wei and Y. Xie, *New J. Chem.,* 2012, **36**, 619.
37 S. D. Zhang, B. Shang, J. L. Yang, W. S. Yan, S. Q. Wei and Y. Xie, *Phys. Chem. Chem. Phys.*, 2011, **13**, 15873.
38 C. Z. Wu, X. D. Zhang, J. Dai, J. L. Yang, Z. Y. Wu, S. Q. Wei and Y. Xie, *J. Mater. Chem.,* 2011, **21**, 4509.